Materials Science and Engineering, A110 (1989) 77–87

Tensile Deformation of Coarse-grained Cast Austenitic Manganese Steels

D RITTEL and I ROMAN

Materials Science Division, Graduate School of Applied Science and Technology, The Hebrew University of Jerusalem, Jerusalem 91904 (Israel)

(Received April 18, 1988; in revised form July 13, 1988)

Abstract

In the present study the inhomogeneous deformation behavior of coarse-grained Hadfield steels on both macroscopic and microscopic scales is summarized. This behavior is described and explained in terms of bifurcation analysis, with special emphasis on the orange-peel phenomenon as an example of bifurcation into surface mode. Beyond the study of a particular steel, the deformation behavior of transitional coarse-grained materials in general is addressed. The hardening characteristics of the material are shown to dictate its deformation behavior and the occurrence of localized modes. Specifically, low strain-hardening (at low strain) of cast Hadfield steel is shown to cause orange-peel formation. However, the inclusion of a microstructural parameter (e.g. grain size) into the bifurcation analysis is required in order to provide a better description of the wavelength of the phenomenon

1. Introduction

Hadfield steels have long been known for their outstanding wear and hardening characteristics [1]. The mechanisms of the unusual strain-hardening behavior of these steels have been extensively studied and attributed to various factors including dynamic strain-aging, twinning and transformation-induced plasticity [2–4]. Most studies were carried out on fine-grained hot-rolled polycrystalline material, and were focussed on microscopic deformation mechanisms.

However, when the average grain size of a material exceeds hundreds of microns so that only a few grains are found in the cross-section of a typical tensile specimen, the material can no longer be considered truly polycrystalline. It exhibits mechanical behavior transitional between that of single-crystals and that of polycrystalline materials [5–12]. In this case, new phenomena such as marked surface rumpling (also known as "orange peel") are observed. Studies of transitional behavior have been performed mostly on aluminum [11, 12]. To our knowledge, no such studies exist on Hadfield steels.

It is also known that large-scale deformation of numerous structural materials involves inhomogeneous localized deformation processes such as the well-known "necking" or shear band formation, which have been analyzed on the basis of continuum plasticity and bifurcation analysis [13–18]. An additional interesting manifestation of inhomogeneous deformation is the occurrence of surface waves, predicted by continuum theory [13], and which are experimentally observed as wrinkles on the surface of pressurized cylinders [19], cracked bending specimens [20] and plane strain tension specimens [21].

The subject of this study is the characterization of inhomogeneous deformation processes occurring in coarse-grained materials, with special emphasis on orange peel in coarse-grained cast austenitic manganese (Hadfield) steel. Macroscopic and microscopic deformation processes are characterized, with emphasis placed on the relationship between continuum plasticity models and actual material behavior, in the spirit of the previous studies cited above.

2. Theoretical background

Before presenting experimental results, some principles of the bifurcation analysis will be briefly outlined. Bifurcation analysis applies to a wide range of phenomena occurring when the plastic deformation of a material departs from homogeneity and concentrates in localized modes, on both the macroscopic (*e.g.* necking) and microscopic scales (*e.g.* shear bands and surface instabilities). Hill and Hutchinson developed

0921-5093/89/$3.50

criteria for the occurrence of bifurcation phenomena for various constitutive relations [13]. For plane strain deformation of an incompressible solid characterized by instantaneous shear moduli μ and μ^*, they showed that no bifurcation can occur as long as the relationships $0 < \sigma < 4\mu^*$ and $\sigma < 2\mu$ are obeyed. Here, σ is the applied stress, μ and μ^* are instantaneous moduli for shear parallel to and at 45° to the tensile axis respectively. For a hyperelastic solid [19], these moduli are given by the following expressions:

$$\mu^* = \tfrac{1}{2}\{Es - (Es - Et)(\cos\alpha + 1/2\sin\alpha)^2 \times (1 + 1/2\sin 2\alpha)^{-1}\} \quad (1)$$

$$\mu = \tfrac{1}{3} Es q \quad (2)$$

In these expressions, Et and Es are the uniaxial tangent and secant moduli respectively. The angle α is fixed and it defines the relative magnitude of the principal strain components. For instance, for an incompressible solid loaded parallel to the direction 2, $\varepsilon_2 = X\cos\alpha$ and $\varepsilon_3 = X\sin\alpha$ where X increases monotonically from zero. For the case of a plane deformation, *e.g.* restricted to the 1–2 plane, the parameter q equals $(\varepsilon_1 - \varepsilon_2)\coth(\varepsilon_1 - \varepsilon_2)$, and the critical stress for bifurcation, σ_2, is given by the following expressions [17, 19]. For small γ

$$\frac{\sigma_2}{4\mu^*} = 1 + \frac{1}{3}\gamma^2 + \frac{7}{45}\gamma^4 + 0\left(\gamma^6 \frac{\gamma^6 \mu^*}{\mu}\right) \quad (3)$$

For $\gamma \to \infty$

$$\frac{\sigma_2}{2\mu} = 2\left(\frac{\mu^*}{\mu}\right) + \frac{\sigma}{2\mu}\left(\frac{1 - \sigma/2\mu}{1 + \sigma/2\mu}\right)^{1/2} \quad (4)$$

Here, $\gamma = (m\pi h)/l$ where h and l are the specimen half-width and half-length respectively, and m is an integer. Equation (3) describes the long-wavelength mode (*e.g.* necking), whereas eqn. (4) describes the short-wavelength surface mode. For a plane strain deforming material, *i.e.* $\alpha = 0$, these results have been summarized for various regimes of the equilibrium equations (elliptic, hyperbolic and parabolic) by Tvergaard *et al.* [17] (Fig. 1). For a material whose plastic flow is described by a uniaxial power law, the following relationships are established for the plane strain configuration:

$$\frac{\mu^*}{\mu} = \frac{Et}{Es}\frac{1}{q} = \frac{n}{q} \quad (5)$$

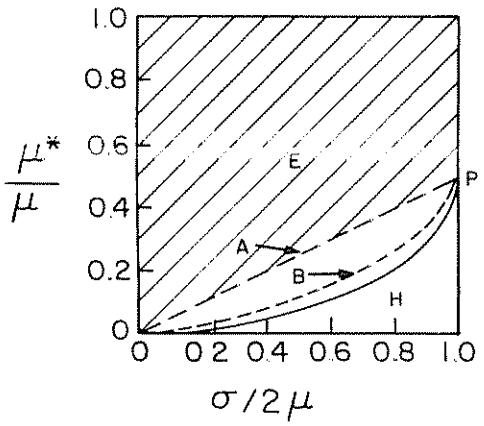

Fig. 1 Bifurcation analysis. Schematic plot showing E(lliptic), P(arabolic) and H(yperbolic) regimes for an incompressible material in plane strain tension. A indicates bifurcation past maximum load (long wavelength), and B indicates the short-wavelength mode limit. Bifurcation is excluded in the hatched area. (Reprinted with permission from ref. 17.)

$$\frac{\sigma_2}{2\mu} = \frac{2\varepsilon_2}{q} \quad (6)$$

where n is the strain-hardening exponent. It is worth mentioning that the hypoelastic solid of Stören and Rice [22] is characterized by $q = 1$ [17]. In this case, employing relationships (5) and (6), the interpretation of Fig. 1 is quite clear for materials with constant n: when the hardening exponent n is plotted as a function of twice the value of the axial strain, 2ε, the sequence of bifurcation events is easily predictable as the various bifurcation domains are entered with increasing strain.

By contrast, for the most commonly employed case of uniaxial tensile testing of cylindrical specimens (axisymmetric deformation), much less work has been carried out. A bifurcation analysis for the onset of necking can be found in the work of Hutchinson and Miles [23], who do not discuss surface modes.

3. Experimental details

One heat of cast austenitic manganese steel of the composition shown in Table 1 was employed. The steel was cast into keel blocks in order to ensure soundness. Carbides were dissolved by heating to 1050 °C, followed by quenching in water at room temperature. The resulting microstructure (Fig. 2) is austenitic, with grain sizes ranging from hundreds of microns to millimetres. Dendritic segregation is observable after repeated

TABLE 1 Composition of alloy investigated

Element	C	Mn	Si	P	S	Cr	Ni	Fe
wt %	1.25	13.1	0.47	0.03	0.008	0.13	0.1	Balance

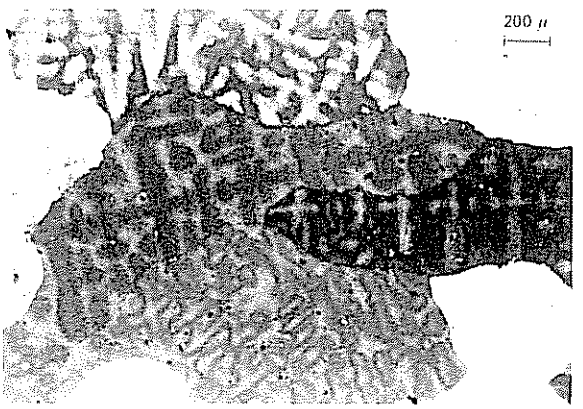

Fig 2. Typical microstructure of coarse-grained Hadfield steel: etchant, Nital (3%)–sodium metabisulfite (10%)

etching and is characteristic of the cast material. Round tensile specimens (8 mm in diameter) were machined from the bottom of the keels. Final dimensions were obtained by fine grinding in order to minimize the formation of a surface hardened layer. Tensile testing comprised an average population of ten specimens and was performed on a closed-loop servo-hydraulic machine under load control (10^4 N min^{-1}) at ambient temperature in air. Initial straining of the specimen, up to 0.01 total strain, was monitored by means of a longitudinal extensometer attached to the specimen. The extensometer was then removed without unloading and testing was continued until fracture. Load–extension (strain) curves were converted to engineering and true stress–strain curves, employing conventional methods. A few tests were carried out under stroke control, and in some cases specimen deformation was video recorded. The total elongation and reduction in area were determined from gauges marked on the specimen and by measurements of the average specimen diameter after fracture respectively.

4. Results

4.1. Mechanical behavior

Yield and fracture strength ranged from 365 ± 25 MPa and from 1410 ± 170 MPa respectively, with a tensile elongation of 0.39 ± 0.06 and a reduction in area of 0.43 ± 0.04. These values indicate the high strain-hardening capacity which characterizes Hadfield steels. The load–extension plots obtained under load control were rather smooth, whereas under stroke control, plastic flow was observed to be highly serrated. Characteristic plots of true stress *vs.* true plastic strain (load control) are shown in Fig. 3 on linear and logarithmic scales. Neither a decrease

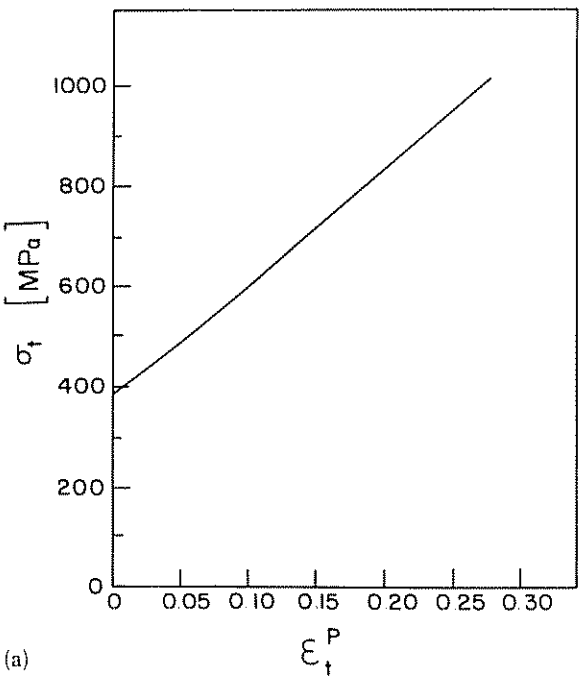

(a)

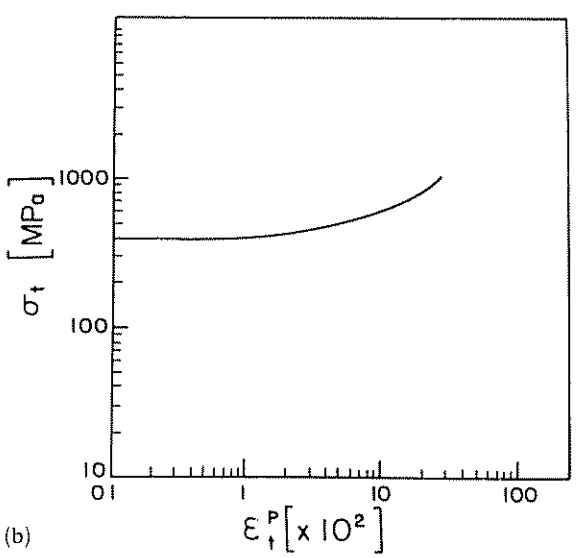

(b)

Fig 3. Typical true stress–true plastic strain behavior of Hadfield steel: (a) linear scale; (b) logarithmic scale

in load nor a neck-like tensile instability occurred during the entire plastic deformation until final failure. Thus the traditional concept of ultimate tensile strength is not applicable here and is replaced by fracture strength, as reported above. From the logarithmic plot, the strain-hardening exponent (slope of the curve) is seen to increase rapidly with strain, and the resulting flow curve is concave upward.

4.2. Macroscopic observations

Visual examination and video recording of the specimen during tensile loading indicated that marked surface rumpling commenced immediately after yield. This phenomenon occurred simultaneously all over the gauge length, seeming to reach macroscopic saturation shortly before final failure (Fig. 4). Two degrees of surface rumpling were observed, namely coarse and fine. When the two occurred simultaneously in the same specimen, the fracture was located in the coarser region (Fig. 4).

Examination of the surface of failed specimens revealed the presence of numerous microcracks, several hundred microns long in circumferential direction, which propagated on radial planes roughly perpendicular to the tensile axis (Fig. 5). A detailed report of this phenomenon is presented elsewhere [24]. Video recordings of the deformation process in a region defined by the objective of the camera revealed that once orange peel nucleated, subsequent deformation was discontinuous. In other words, specimen extension proceeded in a discontinuous manner in the field viewed by the objective.

4.3. Microscopic observations

Micrographs taken from typical longitudinal and transverse sections of deformed specimens are shown in Fig. 6. From these, it can be seen that the orange-peel amplitude, *i.e.* the amplitude of the surface undulations, is dictated by individual grains and is due to significant reorientation of unconstrained free surfaces. Close examination of the deformed microstructure (Fig. 6) reveals that the deformation of coarse-grained Hadfield steels is characterized by a profusion of coarse slip markings and twins which are sometimes difficult to distinguish unambiguously by optical metallography. However, the slip bands reappear after repeated polishings of the metallographic sample and are thus characteristic of persistent slip bands [16, 25]. These deformation features, which form at very low strains, are unevenly distributed among neighboring grains

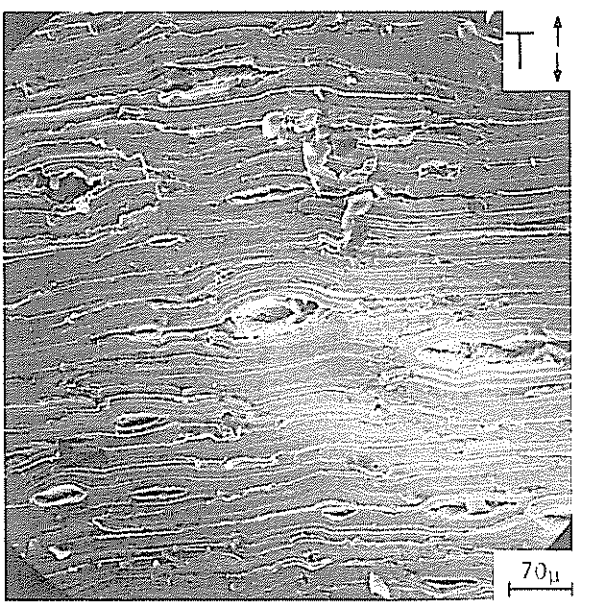

Fig. 5 Scanning electron micrograph showing microcracks on the surface of the deformed specimen (T indicates tensile axis)

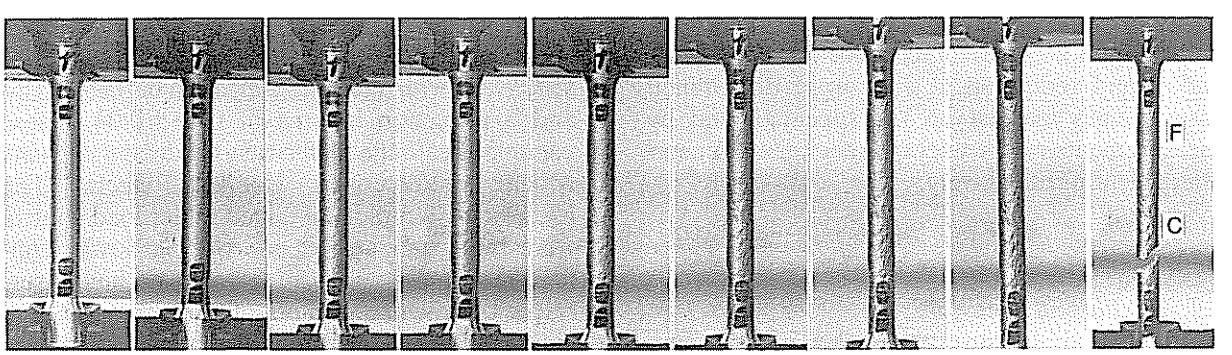

Fig. 4 Orange-peel evolution during straining: C, coarse; F, fine

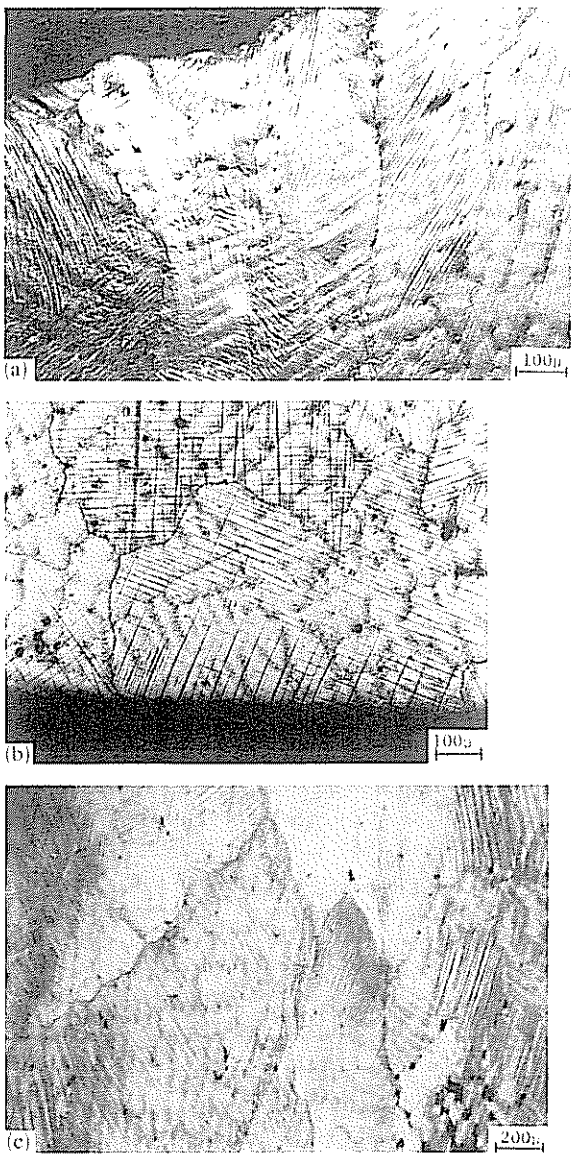

Fig. 6 Typical deformed microstructures (a) Cross-sectional view of a surface grain Orange peel causes free surface undulations (b) Longitudinal section Deformation markings after 0 02 plastic strain (c) Longitudinal section Inhomogeneous distribution of deformation markings after straining to rupture

and within the grains themselves. A higher density of slip markings and twins can be seen in the vicinity of the grain boundaries. Another microscopic feature of the plastic deformation is the presence of shear bands intersecting twin lamellae at an angle of about 36°. This was observed only in grains located in the immediate vicinity of the fracture surface (Fig. 7).

In order to determine local strains in surface grains and their relationship to externally applied

Fig. 7 Longitudinal section of area located below the fracture surface (nickel plated) Shear bands intersect twin lamellae

strains, microgauges were marked by means of microhardness indentations in two locations (Fig. 8): (a) "grain-boundary gauge" located on a grain boundary separating two adjacent grains; (b) "bulk gauge" within the grain. These two types of gauges were applied on the exterior surface of carefully polished and etched specimens. Local plastic strains were determined for both types of gauges from micrographs taken after unloading. The results are shown in Fig. 8, and they indicate that the "grain-boundary strain" is nearly equal to the external strain, whereas the "bulk strain" largely exceeds the latter.

5. Discussion

The experimental results indicate that the deformation of coarse-grained Hadfield steels is characterized by the following features.

(a) Macroscopically: discontinuous extension, orange peel, rapidly increasing strain hardening, lack of necking.

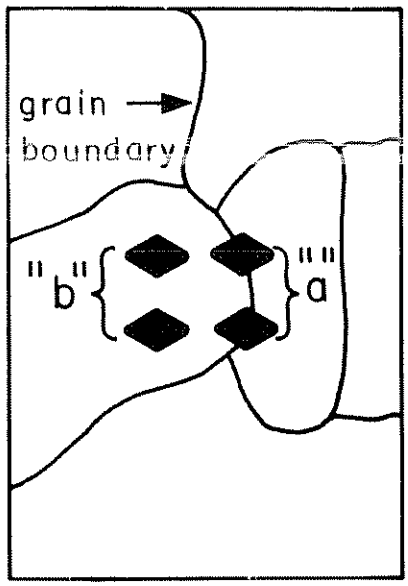

(a)

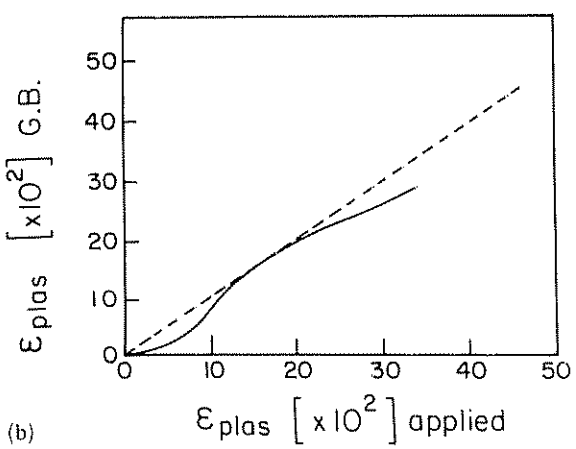

(b)

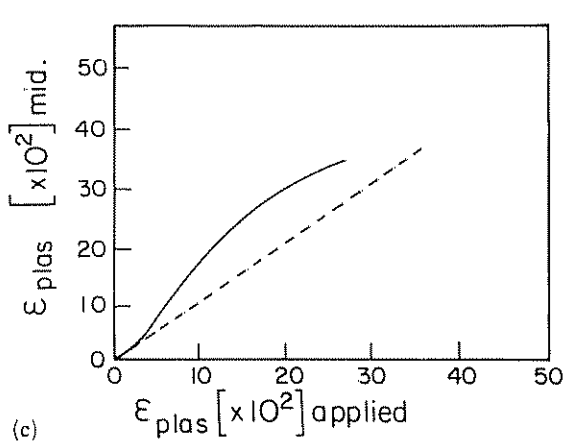

(c)

Fig 8 (a) Location of the microgauges. (b) Plot of the "grain-boundary" plastic strain (ε plas. G.B.) *vs* externally applied plastic strain (ε plas. applied) (c) Plot of the "bulk plastic strain" (ε plas. mid) *vs* externally applied plastic strain

(b) Microscopically: inhomogeneous distribution of deformation markings (twinning, coarse slip bands and shear bands).

The discontinuous extension, as viewed in video recordings, indicates that each grain, or group of grains, deforms separately. The strain is unevenly distributed across the specimen gauge section and plastic deformation proceeds inhomogeneously, immediately after yielding. Dastur and Leslie [3], among others, have reported the serrated character of the plastic flow of Hadfield steels. However, serrated flow may be due to intrinsic microscopic mechanisms, such as dynamic strain aging, and it is not readily observed macroscopically on the specimen, unless special care is exercised. Here we deal with grossly discontinuous extension, as it is observed on the specimen itself rather than on load–extension plots [3]. This behavior is related to the coarse-grain size of our material, which tends to deform as an aggregate of "mechanically-independent" grains. In such a material, the lack of homogeneity becomes macroscopic. These observations stand in contrast with the homogeneous nature of the plastic deformation observed in most engineering materials until the onset of necking. We will discuss the contribution of two important parameters to this behavior, namely the grain size and the hardening characteristics of the material.

5.1. *Grain size effect*

Studies employing coarse-grained aluminum samples have shown that the orange-peel phenomenon stems from reorientation of large unconstrained free surfaces. In the present case, the wavelength of the surface undulation is dictated by the grain size (with an average of a few grain diameters), as noted also by Lewandowski and Thompson [21]. It is also evident that orange peel is not related to entire grains since mid-grain free surfaces are exposed during specimen preparation. The size of these surfaces is randomly distributed as surface grains are randomly cut across, and this effect is particularly obvious for coarse-grained materials. The amplitude of the surface undulation in each individual grain is dictated by the degree of constraint exerted by the closest internal grain boundary. The distance between the surface and the closest internal grain boundary varies randomly, thus yielding a random degree of constraint on the free surface deformation.

Observations of orange peel in coarse-grained aluminum were associated with transitional mechanical behavior characterized by discernible "easy glide" on the stress–strain curves. Such a behavior which involves the grain size and specimen diameter is dictated by the number of grains per stressed cross-section rather than by the grain size itself. The specimens employed in this study contained about ten cross-sectional grains and consequently exhibit transitional behavior characterized by orange-peel formation. This fact was not addressed in previous studies of this material.

On a microscopic scale, the grain size influences the deformation pattern in the sense that coarse grains deform essentially by single slip in regions situated away from the boundaries [5]. It is thus expected that external regions that give rise to the orange peel deform essentially by single slip, whereas in the vicinity of grain boundaries multiple slip is operative as a consequence of compatibility requirements between adjacent grains. It is thus obvious that the deformation pattern is inhomogeneous on a microscale, causing the observed uneven distribution of deformation markings. This lack of microscopic homogeneity is consistent with previous observations of deformation markings in Hadfield steels [3, 4], indicating that in this respect coarse-grained cast material does not markedly differ from finer-grained wrought material. This also means that microscopic deformation characteristics of Hadfield steels are relatively insensitive to microstructural inhomogeneity such as dendritic segregation.

5.2. *Hardening*

True stress–true plastic strain plots show the rapid increase in the strain-hardening exponent from very low initial values (less than 0.1) which steadily increase with plastic strain. The microstructural mechanisms responsible for the high hardening region have been extensively studied, as stated previously, whereas the low strain-hardening region was not considered unusual and consequently deserved no special attention. Nevertheless, some facts stemming from the present work, regarding the nature of strain hardening of Hadfield steels, are worth noting in this specific context of a coarse-grained transitional material.

The observed curvature of the flow curve (first noted by Doepken [2]) is not uncommon for austenitic steels. For these, Ludwigson [26] proposed that the low initial rate of hardening stems from extended planar slip of dislocations, as is the case for low stacking-fault energy material [27]. For Hadfield steel, this energy has been estimated to be in the range of 20–40 mJ m^{-2} [28], which is relatively low. This value is not related to the material condition (cast or wrought) or grain size, so that the previously reported curvature of the flow curve is also observed in the present case. Furthermore, a low initial rate of hardening is likely to result from the extended easy glide which is characteristic of favorably oriented single crystals and transitional polycrystalline materials, as in the present case. An additional contribution to the low initial hardening of the material stems from the reorientation of free surfaces, which is associated with orange peel. This reorientation probably counteracts grip constraint effects [29], at least during the initial stages of the deformation.

Although a unique value of the strain-hardening exponent is not calculable, its asymptotic values can be roughly estimated. It appears that for a plastic strain range of 0–0.1, the hardening exponent does not exceed 0.1, whereas for a plastic strain range of 0.1 to fracture, this exponent increases rapidly with strain and reaches values of up to 0.7 at fracture. These values can be compared with those found in the work of Dastur and Leslie, in which n was found to increase from 0.2 at 0.02 strain to 0.6 at 0.25 strain. It is evident that markedly lower initial hardening exponent values are measured in the present case. This trend can be attributed, among other factors, to the transitional mechanical character of this material, as emphasized above.

An additional characteristic of the inhomogeneous deformation of Hadfield steels is the lack of tensile necking despite the high ductility of this material. Various criteria have been developed for the onset of necking [23, 30]; for power-law hardening material, necking occurs simply when $\varepsilon = n$. In the low strain range, this condition is not obeyed since the value of the hardening exponent exceeds that of the plastic strain, and deformation proceeds inhomogeneously from the onset of yielding.

The hardening exponent was determined for small strain intervals by numerical differentiation of true stress–true plastic strain curves, and the results are summarized in Fig. 9. These results were calculated for two specimens, one strained

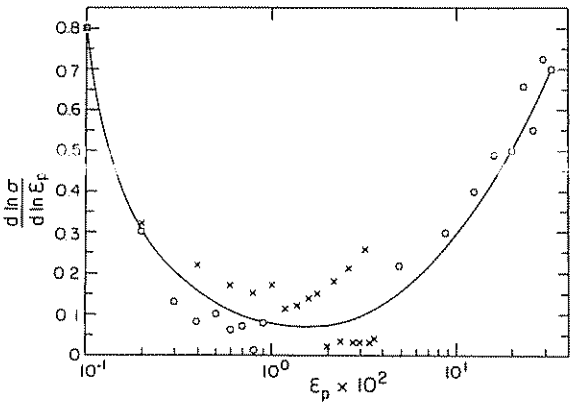

Fig 9 Plot of the strain hardening exponent vs plastic strain The two different kinds of symbol stand for two specimens

in the low strain region, the other strained to fracture. Despite fluctuations in calculated values, the following trend is observed: the region corresponding to very small plastic strain (0.001–0.002) is characterized by a high hardening exponent, whereas for strains up to 0.05 the calculated values are quite low. Further straining causes increasingly high values, as expected. The present results are in qualitative accord with those of Adler *et al.* [4] who focussed on the mechanisms responsible for the hardening of coarse-grained wrought Hadfield steel, and this subject is not our main concern. However, it is worth mentioning that such high initial hardening at very low plastic strains may merely result from elastic behavior. Consequently, this transition region will not be discussed further.

Before drawing quantitative conclusions from such results, the validity of the true stress–true plastic strain relationship should be carefully re-evaluated for the case where significant surface alterations develop, such as orange peel. The instantaneous cross-section of the specimen is subject to large variations, according to the amplitude of the surface waves. Moreover, we showed that the local microscopic strain in the surface regions exceeds the macroscopic strain. Consequently, in such a case, the true stress–true plastic strain curve is only indicative of the average mechanical response of the material, and it does not accurately reflect local behavior. Keeping this fact in mind, it is evident that actual numerical data shown in Fig. 9 cannot be used in a straightforward quantitative manner. Nevertheless, their general trend is sufficient to explain the various deformation features observed, as discussed next.

5.3. Continuum plasticity and actual material deformation behavior

The results of the bifurcation analysis presented in the introduction can be applied to analyze the deformation of Hadfield steels, assuming this material is described by a non-linear elastic (power-law hardening) constitutive relation. As previously stated, this analysis has been widely developed for plane strain deformation, whereas, to our knowledge, no similar complete analysis exists for the case of axisymmetric deformation where the proportionality between the strains is described by $\alpha = -26.56°$. However, Hutchinson and Tvergaard [19] have analyzed the case of surface instabilities for various α and n values (Figs. 2 and 3 in ref. 19). The results indicate that surface instabilities are not restricted to plane strain deformation. They also develop during axisymmetric deformation, and the value of the critical axial strain (ε_2) associated with the bifurcation is minimal for plane strain deformation.

Keeping the distinction between plane strain and axisymmetric deformation in mind, we proceed to analyze our results on the basis of former results obtained for the plane strain configuration. This approximation turns the following analysis into a "lower bound" type of analysis. Here we make use of the strain-hardening exponent throughout the analysis. The reason for this choice is the ambiguous determination of Et from experimental data, whereas the strain-hardening exponent is more familiar to mechanical metallurgists. (For a discussion on the validity of Et as a strain-hardening parameter, see for example ref. 30.) Additional simplification is gained if the value of q is assumed to remain close to unity throughout the relevant strain range. The validity of this assumption, which is equivalent to the hypoelastic model, is easily verified in the plane strain configuration, as q does not exceed 1.15 at fracture. Thus the distinction between hypoelastic and hyperelastic solid is of lesser importance.

With the above simplifying assumptions, the results shown in Fig. 9 can be replotted schematically in Fig. 10 together with the bifurcation domains of Fig. 1. Here the ordinate axis corresponds to the strain-hardening exponent, and the abscissa is twice the axial plastic strain.

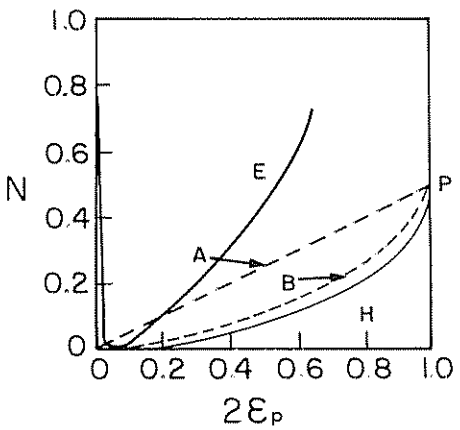

Fig. 10. Schematic plot of the strain-hardening exponent *vs.* plastic strain (Fig. 9) superimposed on bifurcation analysis results (Fig. 1).

From this figure, it is noted that low hardening corresponds to a bifurcation into surface modes in the elliptic regime. Orange-peel formation right after yielding is precisely such a surface mode. As mentioned previously, surface waviness of much smaller wavelength has been observed in various types of specimens (plane strain configuration), and the phenomenon was correlated with a critical strain for bifurcation into surface modes [19, 20]. In the present case where the hardening exponent is low, there is no point in calculating such a critical strain, the value of which is close to zero regardless of the kind of solid studied [17, 20]. Moreover, it is worth emphasizing that contrary to continuum mechanics predictions the wavelength of the surface rumpling is definitely not arbitrary. It is related to the average grain size, namely to a structural parameter as discussed in the work of Hill and Hutchinson [13] and Hutchinson and Tvergaard [19], among others. Therefore orange peel is not only a mere consequence of the coarse-grain size of a deformed material, but it is also an easily observable manifestation of bifurcation of plastic deformation into a surface mode, owing to the low material hardening soon after yield. A parallel can be established with previous observations of surface instabilities in pressurized cylinders [19]. For aluminum ($n=0.1$) cylinders, surface instabilities were observed, whereas this was not the case for copper ($n=0.33$) cylinders, indicating here too the predominant role of material hardening. Another interesting observation is that the character of the surface cracks and their orientation with respect to the surface waves are similar to those reported previously. Although beyond the scope of the present work, it is worth recalling that surface irregularities of this kind are known to trigger other kinds of instabilities such as shear bands which cause ultimate fracture of the specimen [31]. Orange peel gradually disappears with decreasing grain size, corresponding to increased initial strain-hardening [10, 11], so that it is not observed in true polycrystalline material. Lastly, orange peel is an interesting example of low strain bifurcation into a surface mode which precedes necking (absent in our case), to be contrasted with the more commonly observed case where necking occurs before surface deformation (if any) [17]. This mode, which is predictable from the existing plane strain analysis, is actually observed for axisymmetric deformation (present case). This suggests therefore that the critical parameter is the hardening of the material, as it is well known to metallurgists that orange-peel development is not restricted to one precise type of deformation.

Further bifurcation in the form of shear band formation is possible only after entering the hyperbolic regime in the low strain–low hardening part of the deformation history. This regime begins approximately at a plastic strain of 0.1. Owing to the curvature in the hardening characteristics of the material, this domain is not reached, and no shear bands are expected or observed at this stage.

The high strain–high hardening region is located in the elliptic regime where no additional bifurcations can occur. In this regime the deformation concentrates microscopically in coarse slip bands. Lastly, it is suggested that the observation of shear bands (similar to those reported for aluminum alloys [32, 33]) located in the vicinity of the fracture plane can be qualitatively correlated to bifurcation in the parabolic regime for some individual heavily strained grains.

Some general conclusions beyond the case of Hadfield steels can be drawn from this study. First, the bifurcation phenomena which are often associated with high strains [31] are primarily dependent on the hardening characteristics of the material. These characteristics are dictated by numerous microstructural parameters including coarse-grain size and low stacking fault energy among other factors. These factors cause transitional mechanical behavior, yielding the observed orange peel as an example of surface deformation associated with low strain. Consequently, it is felt that analyses similar to ours and to others, aimed

at correlating continuum plasticity to actual material behavior (for example, refs. 18 and 20), should provide additional insight into the deformation of structural materials and its control by metallurgical means, ultimately yielding improved fracture properties.

6. Conclusions

The tensile deformation of coarse-grained cast austenitic manganese steel has been characterized and compared with previous results on wrought fine-grained material. The deformation was observed to be inhomogeneous on both macroscopic and microscopic levels. The microscopic deformation features of the coarse-grained cast material were found to be identical with those reported for fine-grained wrought material. These features are therefore characteristic of the material, regardless of its condition (cast or wrought), grain size and microstructural homogeneity. On the macroscopic level, the material extends in a discontinuous manner and thus behaves as an aggregate of "mechanically independent" grains. Another characteristic deformation feature is the formation of orange peel immediately after yielding. These results have been analyzed within the framework of the bifurcation analysis for plane deformation, employing the strain-hardening exponent as the critical material property rather than a critical strain. This property is particularly interesting, in the case of Hadfield steels, because it increases continuously with strain (at high strain) instead of remaining constant as is the case for most engineering materials. We focussed on the low hardening region of the material, which had not yet received special attention. Low hardening was shown to be related to the combined influence of the low stacking fault energy and coarse-grain size, both of which cause transitional mechanical behavior. Specifically, this region corresponds to bifurcation of the plastic deformation into surface modes. Using simplifying assumptions, we showed that orange peel is precisely such a surface mode and not a mere consequence of the coarse-grain size. This conclusion applies to the general case of transitional materials, beyond the specific case of Hadfield steels with their characteristic hardening.

However, it is felt that there is still a "missing link" between the bifurcation analysis and the orange-peel phenomenon. The introduction of a microstructural parameter (*e.g.* grain size) would be helpful in relating the wavelength of surface modes to the microstructure. In addition, the analysis should be extended beyond the plane strain case, and these two points provide an exciting challenge for the theoretician.

Acknowledgments

The authors wish to express their gratitude to Urdan Associated Steel Foundries for the generous provision of experimental material and samples. We also greatly acknowledge Professor R. Ghez and Professor D. Durban for useful discussions.

References

1 *Metals Handbook, Vol. 1*, American Society for Metals, Metals Park, OH, 8th edn., 1961, p. 834
2 H. C. Doepken, *J. Met.*, February (1952) 166
3 Y. N. Dastur and W. C. Leslie, *Metall. Trans. A, 12* (1981) 749.
4 P. H. Adler, G. B. Olson and W. S. Owen, *Metall. Trans. A, 17* (1986) 1725
5 R. W. K. Honeycombe, *The Plastic Deformation of Metals*, Arnold, London, 1984
6 M. F. Ashby, *Philos. Mag., 21* (1970) 399
7 U. F. Kocks, *Metall. Trans., 1* (1970) 1121
8 C. Rey and A. Zaoui, *Acta Metall., 30* (1982) 523
9 R. E. Hook and J. P. Hirth, *Acta Metall., 15* (7) (1967) 1099
10 R. L. Fleischer and W. A. Backofen, *Trans. Metall. Soc. AIME, 218* (1960) 243.
11 R. L. Fleischer and W. F. Hosford, Jr., *Trans. Metall. Soc. AIME, 221* (1961) 244.
12 R. L. Fleischer, *Acta Metall., 9* (1961) 184
13 R. Hill and J. W. Hutchinson, *J. Mech. Phys. Solids, 23* (1975) 239.
14 J. R. Rice, *Theoretical and Applied Mechanics*, North-Holland, Amsterdam, 1977, p. 207
15 R. J. Asaro, *Acta Metall., 27* (1979) 445
16 Y. W. Chang and R. J. Asaro, *Acta Metall., 29* (1981) 241
17 V. Tvergaard, A. Needleman and K. K. Lo, *J. Mech. Phys. Solids, 29* (1981) 115
18 L. Anand and W. A. Spitzig, *Acta Metall., 30* (1982) 553
19 J. W. Hutchinson and V. Tvergaard, *J. Mech. Phys. Solids, 22* (1980) 339
20 O. A. Onyewuenyi and J. P. Hirth, *Metall. Trans. A, 13* (1982) 2209.
21 J. E. Lewandowski and A. W. Thompson, *Metall. Trans. A, 17* (1986) 461
22 S. Stören and J. R. Rice, *J. Mech. Phys. Solids, 23* (1975) 421.
23 J. W. Hutchinson and J. P. Miles, *J. Mech. Phys. Solids, 22* (1974) 61.
24 D. Rittel and I. Roman, *Metall. Trans. A, 19* (1988) 2269

25 R. J. Price and A. Kelly, *Acta Metall.*, *12* (1964) 979
26 D. C. Ludwigson, *Metall. Trans.*, *12* (1971) 2825
27 L. Murr, *Interfacial Phenomena in Metals and Alloys*, Addison-Wesley, Reading, MA, 1975
28 W. N. Roberts, *Trans. Metall. Soc. AIME*, *230* (1964) 372.
29 J. Hauser and K. A. Jackson, *Acta Metall.*, *9* (1961) 1.
30 W. J. MacGregor Teggart, *Elements of Mechanical Metallurgy*, Collier-Macmillan, London, 1966.
31 N. Tryantafyllidis, *Int. J. Eng. Sci.*, *8* (1984) 1187.
32 K. Morii, H. Mecking and Y. Nakayama, *Acta Metall.*, *23* (1985) 379.
33 J. E. King, C. P. You and J. F. Knott, *Acta Metall.*, *29* (1981) 1553.